Cerebral Cortex, January 2021;31: 169–183

doi: 10.1093/cercor/bhaa218
Advance Access Publication Date: 27 August 2020
Original Article

ORIGINAL ARTICLE

Decision Signals in the Local Field Potentials of Early and Mid-Level Macaque Visual Cortex

Aravind Krishna[1,2], Seiji Tanabe[1] and Adam Kohn[1,3,4,]

[1]Dominick Purpura Department of Neuroscience, Albert Einstein College of Medicine, Bronx, NY 10461, USA, [2]Department of Bioengineering, School of Chemical and Biotechnology, SASTRA University, Thanjavur 613401, India, [3]Department of Ophthalmology and Visual Sciences, Albert Einstein College of Medicine, Bronx, NY 10461, USA and [4]Department of Systems and Computational Biology, Albert Einstein College of Medicine, Bronx, NY 10461, USA

Address correspondence to Adam Kohn, Albert Einstein College of Medicine, 1410 Pelham Parkway South, Room 822, Bronx, NY 10461, USA. Email: adam.kohn@einsteinmed.org

Abstract

The neural basis of perceptual decision making has typically been studied using measurements of single neuron activity, though decisions are likely based on the activity of large neuronal ensembles. Local field potentials (LFPs) may, in some cases, serve as a useful proxy for population activity and thus be useful for understanding the neural basis of perceptual decision making. However, little is known about whether LFPs in sensory areas include decision-related signals. We therefore analyzed LFPs recorded using two 48-electrode arrays implanted in primary visual cortex (V1) and area V4 of macaque monkeys trained to perform a fine orientation discrimination task. We found significant choice information in low (0–30 Hz) and higher (70–500 Hz) frequency components of the LFP, but little information in gamma frequencies (30–70 Hz). Choice information was more robust in V4 than V1 and stronger in LFPs than in simultaneously measured spiking activity. LFP-based choice information included a global component, common across electrodes within an area. Our findings reveal the presence of robust choice-related signals in the LFPs recorded in V1 and V4 and suggest that LFPs may be a useful complement to spike-based analyses of decision making.

Key words: beta, choice analysis, gamma, perceptual decision making, visual discrimination

Introduction

A central question in systems neuroscience is how the activity of sensory neuronal populations relates to our perceptual experience. One approach to answering this question is to record from sensory neurons while animals perform a perceptual task and to relate the measured responses to the animals' reports (Britten et al. 1996). Numerous studies have shown that trial-to-trial fluctuations in individual sensory neurons are correlated with perceptual reports (Parker and Newsome 1998: Nienborg et al. 2012; Seidemann and Geisler 2018). However, although percepts arise from the activity of large neuronal populations, almost all studies exploring this relationship in macaque visual cortex have relied on recordings from single neurons (but see Chen et al. 2006; Bondy et al. 2018; Jasper et al. 2019).

Here, we explore the usefulness of an indirect measure of population neuronal activity—the local field potential (LFP)—for studying the neural basis of perceptual decision making. LFPs are low-frequency, extracellular voltage fluctuations, which arise from summed spiking and synaptic activity (Buzsáki et al. 2012; Einevoll et al. 2013).

Several properties of LFPs suggest that they might be useful for studying perceptual decision making. First, in sensory areas, LFPs are tuned for the attributes of a sensory stimulus in a manner consistent with the selectivity of local spiking activity (e.g., Henrie and Shapley 2005; Kreiman et al. 2006; Liu and Newsome 2006; Katzner et al. 2009; Xing et al. 2009; Jia et al. 2011; Ray and Maunsell 2011; Lashgari et al. 2012). This tuning suggests that LFPs are a useful proxy for local neuronal

activity. Second, LFPs can capture weak, broadly shared signals which are difficult to detect in spiking activity (e.g., gamma-modulation of spiking activity; Fries 2009; Jia and Kohn 2011; Jia et al. 2013; Ray and Maunsell 2015). This sensitivity may be important because neural correlates of perceptual decisions in sensory cortex may involve weak but broadly shared "top-down" signals related to expectation (Goris et al. 2017), belief about task structure (Haefner et al. 2016; Bondy et al. 2018), or feedback from decision areas (Nienborg and Cumming 2009). Third, LFPs are easy to record even in chronic implants (Andersen et al. 2014), facilitating the longitudinal study of neural representations underlying perceptual decision making. Finally, different frequency bands of the LFP have been proposed to indicate signal flow across stages of the visual system. Specifically, gamma fluctuations have been associated with feedforward signaling (Fries 2009), whereas either alpha (5–15 Hz; van Kerkoerle et al. 2014; Michalareas et al. 2016) or beta (14–18 Hz; Bastos et al. 2015) fluctuations have been associated with feedback. Assessing decision information in different frequency bands of the LFP provides a way to assess these proposals and, if supported, to infer how decision information might be routed across stages of a sensory system.

On the other hand, LFPs may aggregate signals too coarsely to be useful. LFPs have been shown to reflect neuronal activity within several hundred microns (Katzner et al. 2009; Xing et al. 2009; Dubey and Ray 2016) to many millimeters away from the electrode (Kreiman et al. 2006; Jia et al. 2011; Kajikawa and Schroeder 2011). Since perceptual decisions are thought to involve precise and often opposite weighting of neuronal responses, based on their task-relevance (e.g., tuning curve slope for the task stimuli; Pitkow et al. 2015), the broad spatial summation of LFPs may render them useless for studying the representation of decision signals in sensory cortex.

To assess whether LFPs in sensory cortex contain decision-related information, we recorded these signals from multielectrode arrays implanted in primary visual cortex (V1) and area V4, a midlevel cortical network, of monkeys performing a fine orientation discrimination task.

Materials and Methods

Subjects

We used two adult, male cynomolgus macaques (*Macaca fascicularis*; 7.4 and 6.8 kg). All procedures were approved by the Institutional Animal Care and Use Committee of the Albert Einstein College of Medicine and were in compliance with the guidelines in the National Institutes of Health *Guide for the Care and Use of Laboratory Animals*.

The subjects were first familiarized with a primate chair (Crist Instruments) and then implanted with a titanium headpost. Implantation was performed under isoflurane anesthesia, following strict sterile procedures. A postoperative analgesic (buprenorphine) and antibiotic (enrofloxacin) were provided. Subjects recovered for at least 6 weeks before the initiation of behavioral training.

Task

The primate chair was clamped to the floor and the subject's head was stabilized in front of a calibrated cathode-ray tube monitor (Iiyama; 1024×768 resolution; 100 Hz refresh; 57-cm viewing distance, so that the monitor subtended $40 \times 30°$ of the visual field). Visual stimuli were generated using custom OpenGL software (Expo; sites.google.com/a/nyu.edu/expo), which also controlled the task contingencies. Eye position was recorded using a video eye-tracking system (SR Research) with a sampling rate of 1 kHz.

Animals were trained on a two-alternative forced-choice, fine orientation discrimination task (Fig. 1A). A trial began when subjects fixated on a small bright spot (0.15×0.15 deg^2; 80 cd/m^2), which appeared at the center of the monitor, on a gray background (40 cd/m^2). After a delay of 200 ms, a drifting sinusoidal grating was presented in the receptive field (RF) of the recorded neurons, for 200 ms (4–5° diameter, full contrast, 2 cpd, 6 Hz drift rate). After an additional delay of 200 ms, the fixation spot was extinguished, and two choice targets were presented. When the grating orientation was closer to vertical than horizontal (orientation >45°), correct decisions required a saccade to the top target; orientations closer to horizontal were associated with the bottom target. Subjects were positively reinforced on correct trials with a drop of liquid reward (Crist Instruments); subjects were rewarded randomly with a probability of 0.5 on a trial involving the 45° grating. The reward was doubled when the subject responded correctly on three consecutive trials. Incorrect trials were followed by a short (5 s or less) time out. Trials in which gaze left a $1.4 \times 1.4°$ window centered on the fixation point were aborted and no reward was given.

During recording sessions, we presented gratings of nine different orientations, centered at 45° and chosen to straddle the slope of the psychometric function (35°–55°), plus the two extremes (0° and 90°). We varied slightly the orientations presented in each session, based on the animals' performance in preceding sessions. Specifically, we sought to balance our need for trials at the decision boundary, for trials with slightly offset orientations to estimate accurately the slope of the psychometric functions, and for easy trials (0° and 90° gratings) to maintain the animals' motivation. The probability of presenting a 45° orientation in most sessions was twice that of the other orientations, whose presentation was equally likely.

Recording

Training continued until subjects reached asymptotic performance, defined qualitatively as stable discrimination thresholds over 4–5 behavioral sessions. We then implanted microelectrode arrays (Blackrock Systems) into primary visual cortex (V1) and area V4 (Fig. 1B). Using knowledge of the retinotopic maps in these areas (Van Essen et al. 1984; Gattass et al. 1988), we targeted the arrays in each area to the retinotopic representation at which stimuli had been presented in training. Each microelectrode array had a 6×8 arrangement, with 0.4-mm spacing. Electrodes were 1 mm in length, and most had impedance near 0.3 MΩ at 1 kHz. For LFPs, extracellular voltage signals were filtered between 0.5 and 500 Hz and digitized at 1 kHz (Blackrock Systems). The spiking activity on each channel was also recorded, with a band pass filter 250–7.5 kHz, followed by digitization at 30 kHz.

We mapped the spatial RFs of the sampled neuronal population on the first days of recording, using the measured spiking responses. While subjects performed a fixation task, we presented small gratings (0.5° in diameter, 2 cpd, 6 Hz drift rate, full contrast; 350 ms duration with 50 ms interstimulus interval) at different positions and orientations. We then placed gratings for the behavioral task on the measured aggregate spatial RFs, with

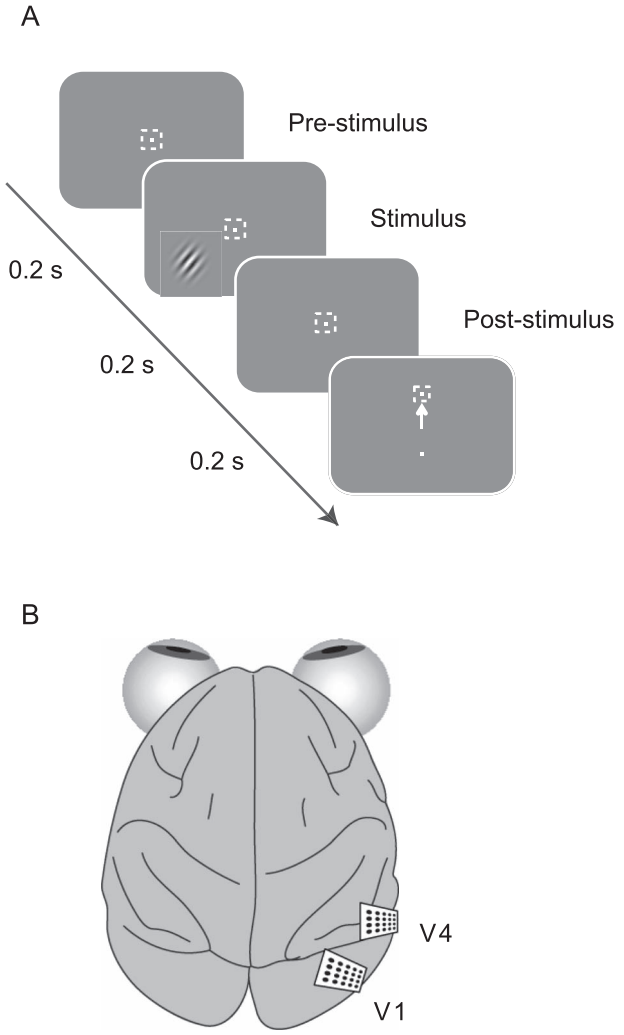

Figure 1. Experimental paradigm. (*A*) Animals were required to fixate a small target in the center of the monitor (white square indicates fixation window; not present on the animals' display). After a delay of 200 ms, a drifting grating appeared for 200 ms. After an additional period of 200 ms, the animal indicated its decision with a saccade to one of two choice targets. (*B*) After behavioral training was complete, we implanted animals with 48 channel microelectrode arrays in V1 and V4.

a diameter sufficient to cover most of the recorded neuronal RFs (4–5°), without impinging on the fixation point. In Monkey 1, the V1 aggregate RFs were at 0.7,−0.3 (elevation, azimuth in degrees of visual angle), and V4 RFs were at 1.6,−1.6. The stimuli were presented at 1.6,−1.6 and had a diameter of 4°. In Monkey 2, the V1 fields were at 2.7,−1.3 and V4 at 3.5,−3. The stimulus was 5° in diameter and was centered at 2.5,−2.5. Subjects were retrained on the behavioral task at the new stimulus location—typically within a few degrees of visual angle of the previously trained location—for approximately a week.

Additional details of the training and recording procedures and the spatial RF maps can be found in Jasper et al. (2019).

Data Analysis

We analyzed only those sessions in which animals' discrimination threshold was $\leq 6°$ and bias was $\leq 3°$, and in which animals provided at least 10 trials of each choice for the 45° stimulus and the two neighboring orientations (60 of 83 sessions). The discrimination threshold was defined as the standard deviation of a cumulative Gaussian function, fit to the behavioral data using the maximum likelihood of a Bernoulli process. The bias was defined as the difference between the mean of the fit function and 45°.

Preprocessing

On some trials, we observed large artifacts in the LFP, likely caused by jaw movements, licking the reward tube, or small body movements. To exclude these contaminated data, we Z-scored the LFP on each electrode and trial and removed cases for which the Z-score exceeded a value of 4 at any point during the trial. We also excluded cases if the peak absolute voltage within individual trials was not between 80 and 500 μV. To prevent any intermittent line noise from affecting our estimates, we also excluded trials if the power at 120 Hz (a harmonic of 60 Hz, chosen to avoid conflation with gamma frequencies) exceeded LFP power in the 0–4 Hz range. If more than 3% of the trials recorded on an electrode were excluded in a session by these criteria, we discarded all data from that electrode for that session. In one of the two animals, we recorded an additional data set from the second hemisphere. In these recordings, the LFP in V1 was often contaminated by artifacts, so this data set was excluded entirely.

We observed some cross-talk between the signals recorded on different array electrodes. This was evident by abnormally high coherence values between high-frequency components of the LFP, exceeding the coherence observed between most pairings. To determine which electrodes were suspect, we measured trial-to-trial LFP coherence across all pairs of electrodes in both V1 and V4 arrays, during the 200-ms epoch before stimulus onset. We flagged pairs of electrodes that had session-average coherence values greater than 0.8 in the frequency range of 70–200 Hz. We then discarded all data from individual electrodes, until all the suspect pairings had been eliminated. In M1, 41.8% of V1 electrodes and 31.8% of V4 electrodes were removed; in M2, less than <0.6% of V1 or V4 electrodes were removed.

We measured the power spectrum and coherency of the included LFPs using multitaper spectral estimation method of the Chronux toolbox (Bokil et al. 2010), with three tapers. We analyzed power for 200-ms epochs of LFP, either before stimulus onset (prestimulus epoch), during stimulus presentation (stimulus epoch), or between stimulus offset and the reporting of choice (poststimulus epoch), unless otherwise noted.

Grand average LFP spectra for each epoch are shown in Figure 2A, separately for each cortical area and animal. Because we estimated power in 200-ms epoch (padded to 256), our spectral resolution was 3.9 Hz. Our analyses used the raw LFP signal; we did not subtract the trial-averaged evoked potential prior to computing LFP power on each trial (i.e., we did not isolate the induced signal). In separate analyses, we found similar results using induced LFP but choice signals were slightly weaker (Supplementary Fig. 1).

Choice Probability

To assess the strength of decision-related activity in the LFP, we computed "choice probabilities" using receiver operator characteristic (ROC) analysis (Britten et al. 1996, see

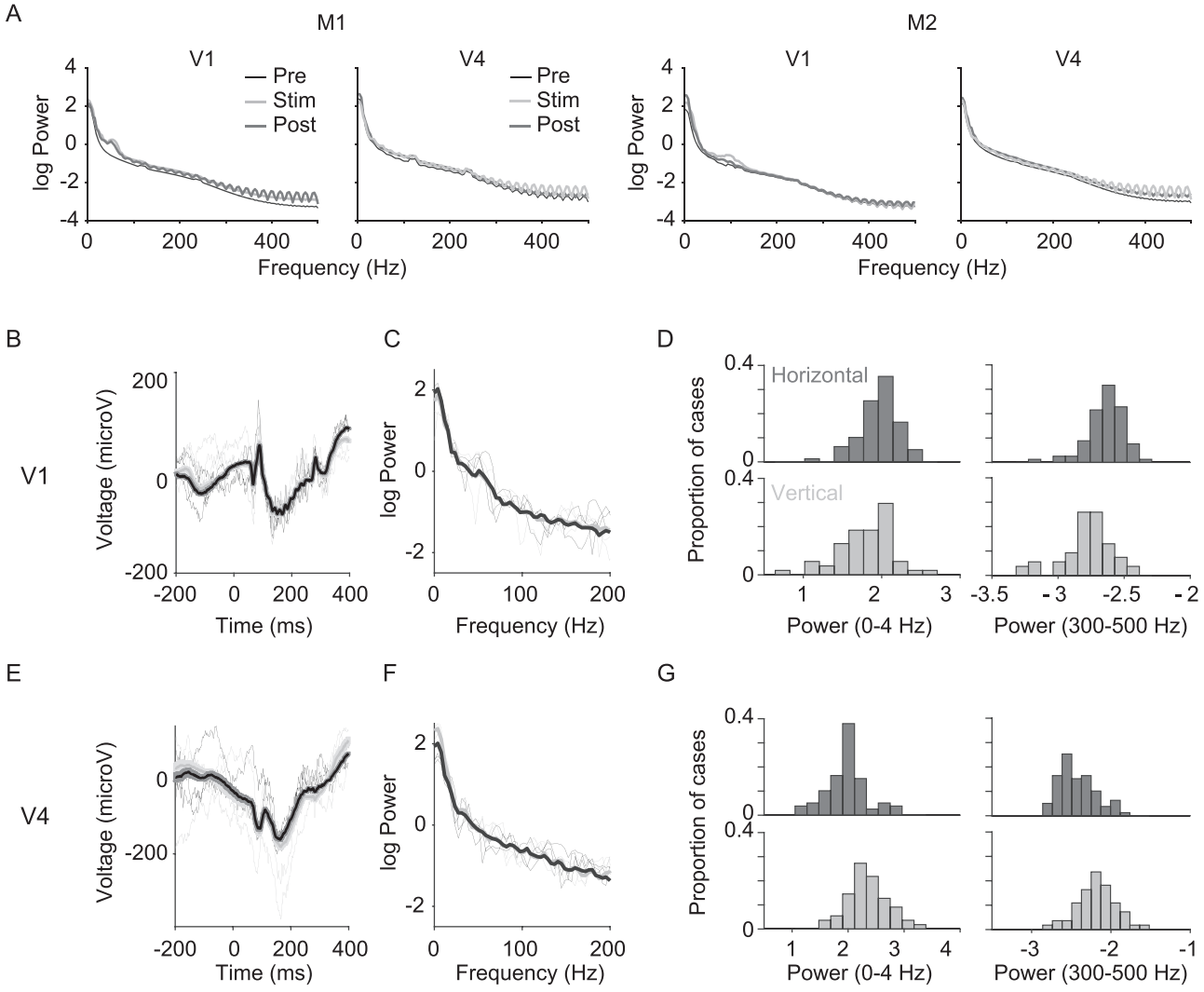

Figure 2. LFP spectra and choice signals. (*A*) Average power spectra for the 45° stimulus computed for each animal and each area, in prestimulus, stimulus, and poststimulus epochs. (*B*) Sample LFPs from a V1 electrode in M1. Trials with horizontal choices are indicated in black; vertical choices in gray. (*C*) LFP spectra for trials with horizontal (black) and vertical (gray) choices. Thin lines show single trial spectra; thick lines show trial-averaged spectra. (*D*) Distributions of power derived from trials with horizontal (dark gray) and vertical (light gray) choices in the 0–4 Hz (left) and 300–500 Hz (right) frequency band. (*E*–*G*) Same as (*B*–*D*), but for a V4 electrode in monkey M1.

Fig. 2*B*–*G*). We first calculated LFP power for each electrode on each trial for the 45° stimulus. We then performed ROC analysis on the distributions of log power for horizontal and vertical choices, after matching the number of trials for the two choices by randomly subselecting trials involving the more frequent choice. This process was repeated five times, using different random selections of trials for the choice for which we had more trials, and the resultant values were averaged to provide better estimates. On average, CP estimates in M1 and M2 were computed with 105 ± 5 and 78 ± 4 trials, respectively. We report the resultant CP values as the absolute deviation from chance (a CP value of 0.5) termed absCP. To assess the probability that the observed absCP arose by chance, we randomly permuted choices across trials and then recalculated absCP from these data, using identical procedures as for the original data. This was repeated 1000 times, and the rank of the measured value in this distribution was used to define the *P*-value. To compare choice information available from spiking responses, we used an identical procedure using spike counts measured in the same time bins.

Population Decoding

To assess the strength of decision signals available from the pool of electrodes, we used logistic regression to predict the monkey's choice from LFP power on each electrode. To increase the number of trials available for fitting, we used responses to the 45° stimulus as well as the two stimuli whose orientation was nearest to 45° (offset by ±1–2°), for which the monkeys' decisions involved a substantial fraction of both choices (at least 10 trials per choice per stimulus). We Z-scored the LFP power for each electrode across trials, separately for each stimulus to remove any stimulus-related signal. We then fit the regression models to the combined data, excluding one randomly chosen trial with a vertical choice and one with a horizontal choice, used to test performance. Model fitting was performed, on average,

with 143 ± 7 and 106 ± 6 trials in M1 and M2, respectively. Each trial was used once for testing, and performance was defined as the average over the cross-validation set. To reduce overfitting, we used Lasso regularization (glmnet for Matlab; Qian et al. 2013), with the strength of the regularization term chosen to minimize model deviance on cross-validation folds within the training set. This process was repeated 10 times, using different random selections of trials for the choice for which we had more trials, and the resultant values were averaged to provide better estimates. We performed a complementary analysis using linear discriminant analysis and obtained similar results (Supplementary Fig. 2).

Similarly, to estimate stimulus-related information, we trained logistic regression models to discriminate responses to the 45° stimulus from the responses to stimuli with offset orientations. Responses were measured in a 200-ms epoch beginning at stimulus onset. Since the orientations presented in each session varied slightly, we binned performance based on the rank order of the orientation offset from the 45° grating: the nearest offset orientation was on average offset by 1.5 ± 0.1°, followed by 3.1 ± 0.1°, 5.5 ± 0.1°, and 45°. For each electrode, we combined responses (i.e., the spectra of the LFP responses) across pairs of stimuli (e.g., 45° and 47°) and Z-scored. We did so to eliminate differences in the power across electrodes while maintaining the difference in power for each stimulus pairing on a given electrode. We matched the number of trials for each stimulus condition by randomly subselecting trials for the stimulus that was shown more frequently. We then used the same fitting approach (i.e., regularization and cross-validation) as for the choice models. To compare choice and stimulus information available from individual electrodes, we trained logistic regression models on single-electrode data, in the same way as for the population decoding.

Using an approach identical to that described in Jasper et al. (2019), we found nearly indistinguishable results to those reported here when we excluded trials in which microsaccades were made within the fixation window during stimulus presentation.

All indications of variance are standard error of the mean unless specified otherwise. All statistical tests were performed using the Wilcoxon signed-rank test, unless otherwise noted.

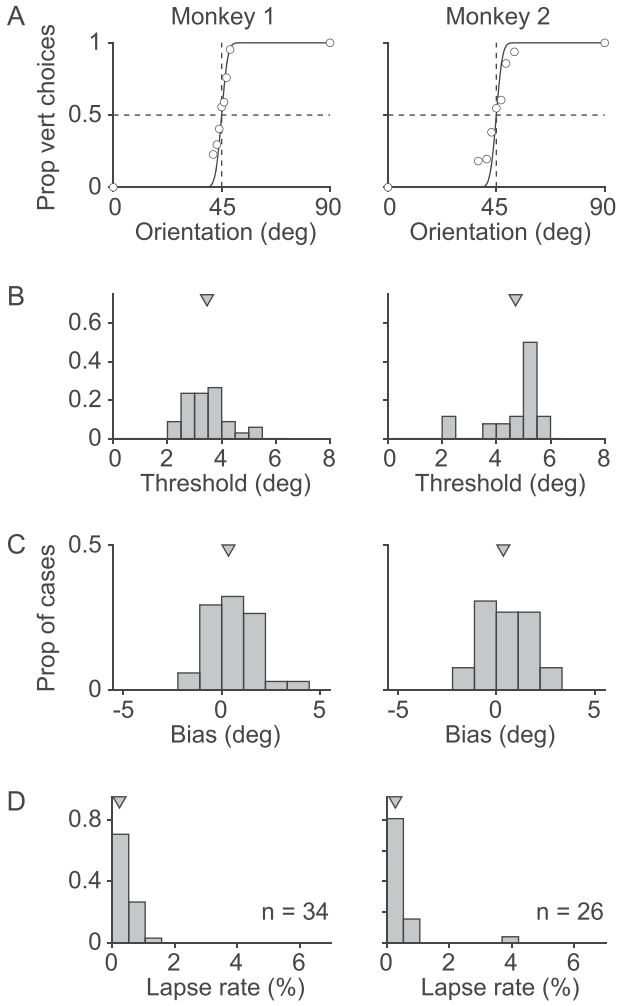

Figure 3. Behavioral performance. (*A*) Psychometric functions for example sessions, for each animal. Circles indicate the grating orientations used and corresponding choices. Lines indicate fits of a cumulative Gaussian function. (*B*) Thresholds for all sessions analyzed, defined as the standard deviation of the function fit to the data. (*C*) Biases for all sessions. Bias was defined as the offset from 45° of the fit function. (*D*) Lapse rate, defined as the percentage of wrong choices for the 0° and 90° stimuli.

Results

We recorded LFPs and spiking activity simultaneously from two 48-channel microelectrode arrays implanted in areas V1 and V4 of monkeys trained to perform a fine orientation discrimination task (Fig. 1A). An analysis of choice signals in the recorded spiking activity is provided in Jasper et al. (2019).

The task required deciding whether the orientation of a briefly presented grating (duration 200 ms, presented 200 ms after fixation) was greater or less than 45°. Decisions were reported by a saccade to a choice target, presented 200 ms after grating offset. Grating orientations were chosen to span the psychometric function; its size was chosen to cover the spatial RFs of the recorded neuronal population.

As shown for example sessions (Fig. 3A), psychometric functions had a steep slope near the decision boundary of 45°, with negligible lapse rate and bias. We quantified subjects' performance in each session by fitting the psychometric function. On average, thresholds were 3.46° ± 0.74° and 4.97° ± 1.23° for the two animals (Fig. 3B), lapse rates were <0.5% (Fig. 3C), and biases were <1.3° (Fig. 3D). Thus, subjects' choices were strongly related to the stimulus orientation, and their performance was comparable to human observers (Mäkelä et al. 1993; Schoups et al. 1995; Mareschal and Shapley 2004; Goris et al. 2017).

We analyzed sessions for which behavioral performance met our inclusion criteria (see Materials and Methods), yielding data from 34 recording sessions in one animal (M1) and 26 sessions in the other (M2). On average, we obtained usable LFP signals from 30.4 ± 1.7 electrodes in V1 (M1: 19.1 ± 0.5, M2: 45.1 ± 0.2) and 27.4 ± 1.0 in V4 (M1: 20.5 ± 0.5, M2: 36.4 ± 0.2; see Materials and Methods for selection criteria). In total, the data set included 22 729 and 12 084 behavioral trials in M1 and M2, respectively; of these, 4358 and 2418 were trials in which we displayed the 45° stimulus.

Choice Signals in the LFP

To assess whether the LFP carries information about the subjects' choices, we compared the frequency composition of the LFP on vertical- and horizontal-choice trials. We first quantified

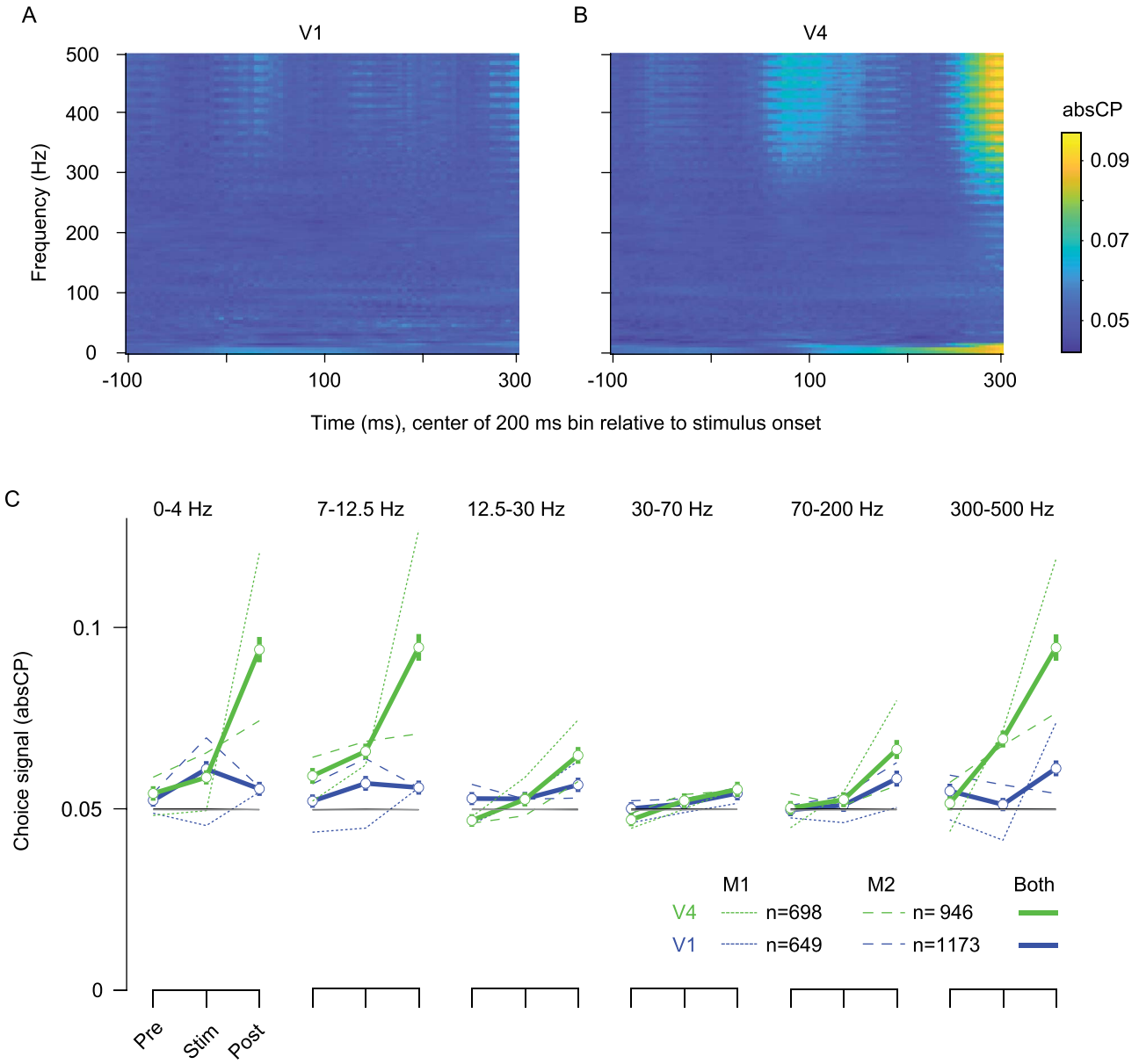

Figure 4. LFP-based choice signals, as a function of frequency band, area, and duration of the trial. (*A*) V1 absCP values, as a function of frequency (ordinate) and time (abscissa). Time label indicates the center of 200 ms bin used to compute the power spectrum, relative to stimulus onset. AbsCP values have been aggregated over the two animals. (*B*) Same as (*A*) but for V4. (*C*) AbsCP values as a function of area (V1 in blue, V4 in green), task epoch (prestimulus, stimulus, and poststimulus), and frequency band. Dotted lines correspond to the data from monkey 1; dashed lines the data from monkey 2. Solid lines indicate the aggregated data. Error bars (SEM) are shown only for the aggregate data to reduce clutter. Black and gray lines indicate the 95th percentile value of absCP values for V1 and V4, respectively, computed from aggregate shuffled data. Black line is obscured by the gray.

the spectral power of the LFP on each electrode and trial and then performed choice probability (CP) analysis on the distributions of spectral power measured on trials with horizontal compared with vertical decisions (see Materials and Methods and Fig. 2*B*–*G*; Britten et al. 1996; Nienborg et al. 2012). CP measures the probability that an ideal observer could predict the animals' choice from the measured responses. A CP value of 0.5 indicates chance performance. Whether the CP is greater or less than 0.5 depends on the assumed relationship between choice and signal (i.e., whether responses should be stronger at a given site for horizontal or vertical choices, in spike-based analysis typically decided by the preference of the neuron). Since the orientation tuning of the LFP can differ across frequency bands (Liu and Newsome 2006; Berens et al. 2008; Jia et al. 2011), it is difficult to compare raw CP values across frequencies. We thus report the absolute deviation of CP from a value of 0.5—a measure which quantifies the strength of decision-related signal, without assuming a particular relationship to site preference. We refer to this quantity as absCP.

We calculated absCP in two complementary ways. First, we calculated absCP for each frequency bin separately, using power measured in sliding epochs of 200 ms, with each window shifted by 5 ms. This provided an unbiased view of how absCP depended on frequency and time (Fig. 4*A*,*B*). Second, to quantify and assess

choice signals statistically, we computed absCP after averaging power in the following frequency bands: 0–4 Hz (low), 7–12.5 Hz (a typical "alpha" range; similar to van Kerkoerle et al. 2014), 12.5–30 Hz (beta, Bastos et al. 2015), 30–70 Hz (gamma, Fries 2009; Jia and Kohn 2011), 70–200 (high gamma; Ray and Maunsell 2011), and 300–500 Hz (sometimes used to measure MUA; Ray and Maunsell 2011; Zanos et al. 2011). For each band, we computed power in three separate epochs, each 200 ms in duration—between the establishment of fixation and the onset of the grating, during stimulus presentation, and between stimulus offset and the appearance of the choice targets (Fig. 4C).

Both views of the data revealed three notable features of LFP-based choice signals.

First, in both V1 and V4, choice information grew in magnitude during the trial. The absCP values were weakest before stimulus onset ("pre" epoch) and strongest in the epoch between stimulus offset and the appearance of choice targets ("post" epoch). For V4, in every frequency bin, absCP values were stronger in the poststimulus epoch than before or during stimulus presentation ($P < 0.001$, no correction for multiple comparisons), except for the gamma band 30–70 Hz ($P = 0.03$). In V1, the poststimulus epoch also had the largest absCP values, at least in the frequency bands with choice information ($P < 0.001$ for comparison to earlier epochs for the two highest frequency bins; $P > 0.05$ for other frequency bins).

Second, choice signals in the LFP were frequency dependent. For instance, in the poststimulus epoch, in V4, absCP magnitude was greatest for frequencies below 12.5 Hz (0.094 ± 0.002 when averaged across the two lowest bands) and above 300 Hz (0.095 ± 0.002), although values were significantly above chance in all frequency bands. Notably, choice-related signal in V4 was particularly weak—nearly at chance—in the gamma range (30–70 Hz, 0.055 ± 0.001; $P < 0.001$ for difference with lower and higher frequencies). In additional analyses, we quantified choice signals in additional frequency bands, in or near the gamma range, where the LFP power spectra showed evidence of enhanced gamma activity (the gamma "bump" as in Jia et al. 2011; Fig. 2). Choice signals were similarly weak in these frequency bands (Supplementary Fig. 3). We also compared the similarity of choice signals in different frequency bands, by assuming a fixed relationship between power and choice across frequencies for each electrode. This revealed that the sign of the choice signal was similar across frequencies (Supplementary Fig. 4).

Third, absCP values were consistently higher in V4 than V1 (compare green and blue traces, Fig. 4). In the poststimulus epoch, when decision signals were most evident, V1 and V4 absCP values were significantly different in every frequency range ($P < 0.001$, no correction for multiple comparison), except for 30–70 Hz ($P = 0.5$). For the 300–500 Hz frequency bin, the mean absCP value in V1 in the poststimulus epoch was roughly 24% greater than the 95th percentile value of performance for shuffled data (black line), whereas in V4, it was 93% greater (0.095 ± 0.002 for V4 vs. 0.061 ± 0.001 for V1, with the 95th percentile of shuffled data being 0.049 for both V1 and V4).

We next compared the dynamics of LFP-based choice signals in V1 and V4 in more detail. We focused on higher frequency components of the LFP, in which choice information was more robust and power could be estimated more accurately for brief epochs. We calculated absCP using the average power between 70 and 500 Hz, measured in sliding 100-ms time windows with 50% overlap. To provide a fair comparison of the temporal evolution of V1 and V4 choice signals, we matched the two areas for performance. Specifically, we subselected an equal number of electrodes in the two areas such that the absCP magnitude distribution in the final 100-ms epoch was the same.

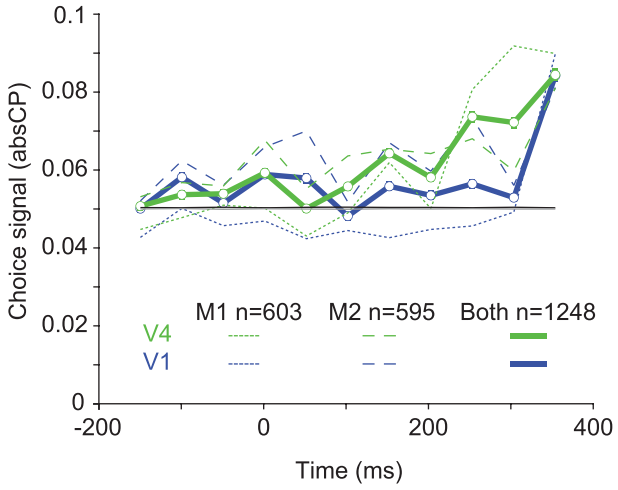

Figure 5. Dynamics of choice information in V1 and V4. absCP values as a function of time, relative to stimulus onset at 0 ms. V1 values are shown in blue; V4 values in green. Dotted lines indicate data from monkey 1, dashed lines from monkey 2. Black line indicates the 95th percentile of absCP values for the aggregate V1 shuffled data; 95th percentile for the V4 data is shown in gray. A number of cases were matched for each monkey and area (*n* values in figure refer to the number of cases in each animal and when distributions were aggregated).

Choice signals were evident in V4 before V1 (green vs. blue, Fig. 5), though the difference was only robust in M1. In V4, average absCP values were significantly greater than in the baseline period (first three 100-ms bins), beginning in the 50–150 ms time window and continuing until the end of the trial (permutation test, 95% confidence interval). In V1, absCP exceeded baseline only after the 100–200 ms time window. The choice signals in V4 were significantly stronger than those in V1, starting in the 0–100 ms window and for all times thereafter, except the last epoch, which was equal by definition ($P < 0.001$, no correction for multiple comparisons). Thus, choice signals are not only stronger in V4 than in V1 (Fig. 4); they are evident in V4 before V1.

Finally, we compared decision-related signal in the LFP to that available from spiking activity, recorded from the same arrays (see also Jasper et al. 2019). Whereas most electrodes had usable LFP signals, only some provided spiking activity (mean 15 ± 8 electrodes out of 48 in each area). To ensure a fair comparison, we only analyzed spikes and LFPs from electrodes on which both signals were available.

On average, LFPs contained more information about choice than spiking activity. In V4, the mean absCP value for spiking activity was 0.051 ± 0.002, in the epoch after stimulus offset. This was significantly smaller than the LFP-based absCP values in the same epoch, for frequency ranges below 30 Hz and above 300 Hz ($P < 0.001$). Similarly, in V1, the mean absCP of spiking activity was 0.045 ± 0.002, which was weaker than the LFP-based absCP in frequency ranges below 30 Hz and above 300 Hz ($P < 0.003$).

Furthermore, we found that the absCP values calculated from LFPs and spiking responses were only weakly correlated. This is illustrated for the high-frequency components of the LFP in Figure 6, which compares the LFP and spike-based absCP values for each electrode in the poststimulus epoch (for V1:

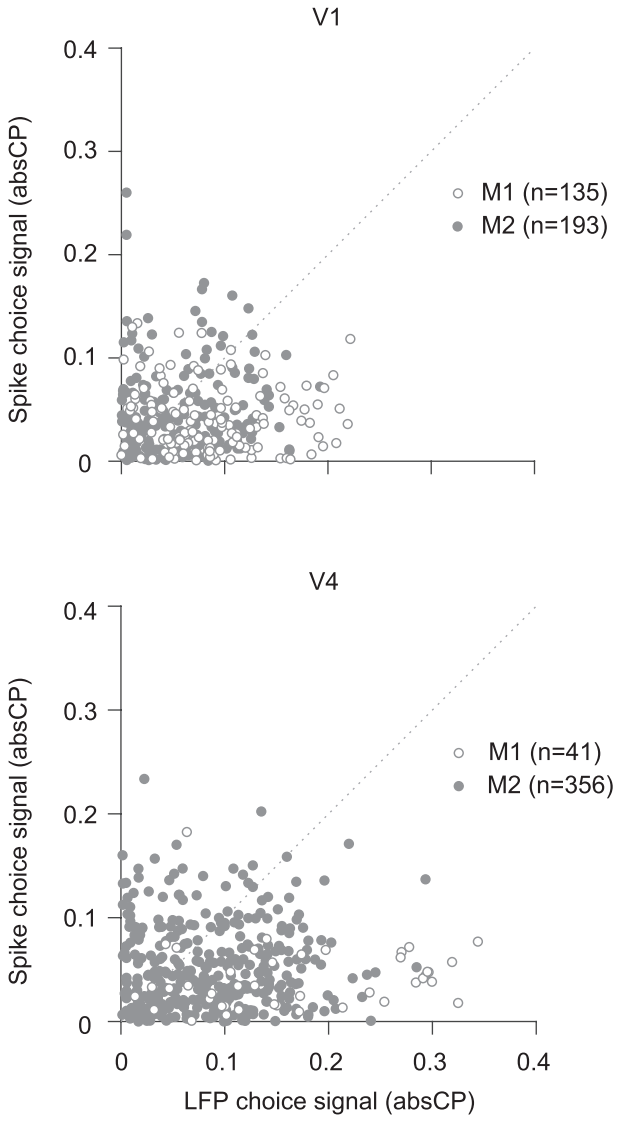

Figure 6. Comparison of choice information in spiking activity and LFPs. The absCP values for spiking activity (ordinate) compared with high-frequency components (300–500 Hz) of the LFP (abscissa), for V1 (top) and V4 (bottom). Each symbol corresponds to data from one electrode in one session; only electrodes on which both spiking activity and LFPs were recorded are included. Open symbols are for data from monkey 1. Filled symbols are from monkey 2. Activity was measured in the poststimulus epoch for both signals.

$r = -0.07$, $P = 0.4$ in M1; $r = 0.07$, $P = 0.3$ in M2; for V4: $r = 0.22$, $P = 0.15$ in M1; $r = 0.04$, $P = 0.4$ in M2; Spearman correlation). Across areas and frequency bins, the correlations between LFP- and spike-based signals were similarly weak (ranging from −0.25 to 0.36, in the poststimulus epoch when both signals were most evident).

We conclude that the LFP contains robust choice-related information in V4 and substantially weaker information in V1. Choice signals are evident across a broad range of frequencies, but weakest in the gamma range (30–70 Hz). Choice signals grow in strength during the trial, appearing in V4 before V1, even after controlling for differences in their strength.

Decoding Choices across Electrodes

We next evaluated how combining LFP signals from multiple electrodes would improve our ability to predict animals' choices. We used a logistic regression model to predict choices using simultaneously recorded signals from either V1 or V4 electrodes. In preliminary work, we found that fitting this decoder to data from all usable electrodes often resulted in overfitting and poor predictions, even with regularization. We thus adopted the alternative approach of decoding from pools of electrodes of increasing number, beginning with the electrode for which the LFP contained the strongest decision signal and adding additional electrodes as determined by their individual decoding performance (assessed separately for each frequency band and time bin). The population size was increased until the cross-validated performance dropped for two consecutive iterations. We then defined the relevant population as that providing maximal performance.

Model performance displayed a similar dependence on area, time epoch, and frequency (Fig. 7), as the single electrode absCP analysis presented previously. First, performance increased during the trial, with weakest performance in the epoch before stimulus onset and maximal performance in the epoch between stimulus offset and the animals' reports. Second, choice could be predicted from both the low- (<30 Hz) and high-frequency (>70 Hz) components of the LFP, in V4. The maximal average performance in V4 was 63.8% in the 300–500 Hz band, and the highest individual session performance was 78.9%, for the 7–12.5 Hz frequency range. Gamma band activity in V4 provided the weakest choice information ($P < 0.0001$, when comparing with other frequency bands except 12.5–30 Hz, $P = 0.19$). Finally, performance was consistently higher for models fit to V4 than V1 LFPs (Fig. 7, green vs. blue; $P < 0.004$). In V1, performance was weak except for the highest frequency band.

Surprisingly, we found that there was often only subtle improvement in model performance for larger pools of electrodes. The most common outcome was that the model performed best with just a few electrodes (see also Supplementary Fig. 2). Information about choice might fail to grow with electrode number because only a few sites contain choice signals. However, our single electrode analysis showed that choice signals were broadly distributed across electrodes (Fig. 6). We propose instead that the choice information in the LFP is highly redundant across electrodes, a possibility we investigate further below.

Relationship between Stimulus and Choice Information

For spiking activity, choice signals are often strongest in neurons that are most relevant to the task (e.g., Britten et al. 1996; Uka and DeAngelis 2004; Purushothaman and Bradley 2005; Nienborg and Cumming 2009; Liu et al. 2013; Pitkow et al. 2015), though in some studies this relationship is weak or absent (Nienborg and Cumming 2006; Price and Born 2010; Shiozaki et al. 2012; Hass and Horwitz 2013; Jasper et al. 2019). We therefore assessed whether choice signals were stronger in LFPs that also conveyed more information about stimulus orientation.

We first evaluated whether V1 and V4 LFPs encoded task-relevant information. We trained a decoder to distinguish between the 45° grating and those with offset orientations, based on the LFP power measured at each electrode during the trial epoch when gratings were presented. We used the

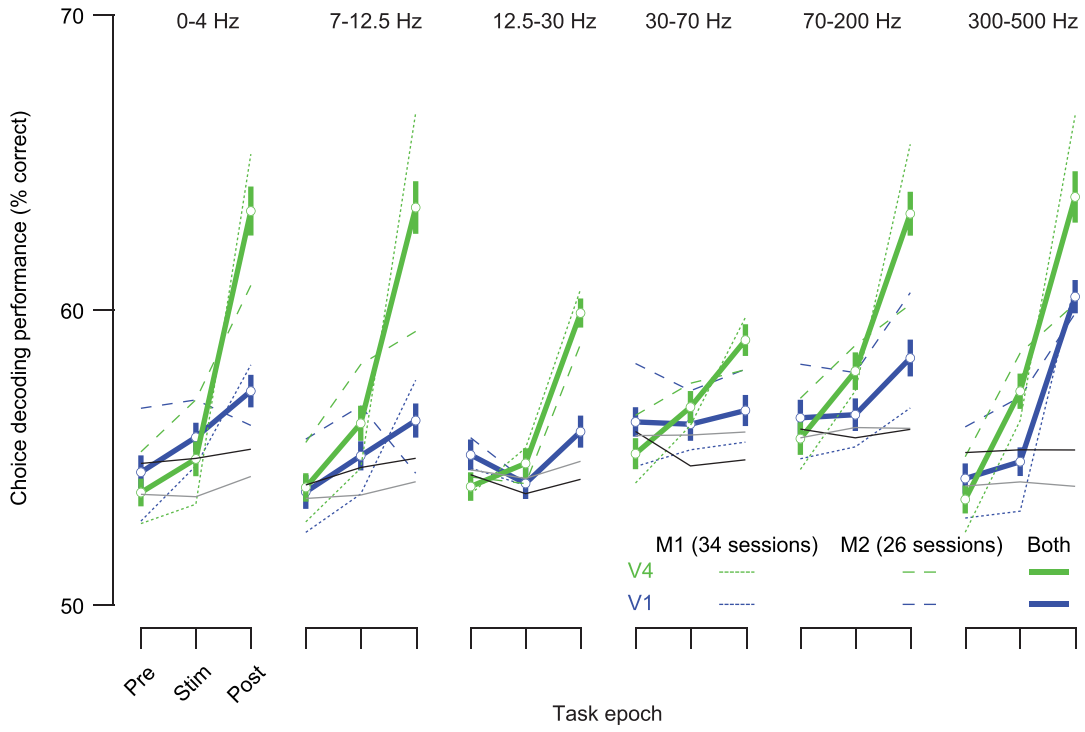

Figure 7. Predicting choice by decoding LFPs from multiple recording sites. Each set of lines shows decoding performance (cross-validated) in predicting animals' choices, for a different frequency band. Blue lines indicate data from V1; green lines from V4. Dotted and dashed lines indicate data from monkeys 1 and 2, respectively; solid lines indicate the aggregated data. Gray, black lines indicate the 95th percentile performance values of a decoder fit to the aggregate shuffled data (for V1 and V4 respectively; using 40 shuffles).

same approach for this analysis as we had to decode choice signals.

Both V1 and V4 LFPs contained robust stimulus information (Fig. 8). For instance, for discriminations of $5.5 \pm 0.2°$, performance ranged from 55.5% to 68.0% in V1 and 54.9% to 60.9% in V4. V1 outperformed V4 with an average difference in the performance of 8.2 ± 2.2 percentage points, except in gamma and high gamma frequencies.

To determine whether the LFPs encoding the most stimulus information were also most informative of choice, we compared choice and stimulus information on an electrode-by-electrode basis. We quantified choice and stimulus information as the cross-validated decoding performance of each electrode, using power measured during the poststimulus epoch for choice and in the stimulus epoch for stimulus information. For the high-frequency range 300–500 Hz, illustrated in Figure 9, we found little relationship between performance for choice and stimulus discrimination (Spearman's correlation in V1: $r = 0.04$ $P = 0.29$ for M1; $r = 0.07$, $P = 0.01$ for M2; in V4: $r = 0.0008$, $P = 0.98$ for M1; $r = 0.01$, $P = 0.66$ for M2). The relationship was also weak or entirely absent in other frequency bands (correlation values ranged from −0.12 to 0.07 across areas, animals, and frequency bands).

We conclude that there is little relationship between the stimulus- and choice-related information available in the LFPs. Sites that were particularly informative about stimulus orientation were not consistently better at predicting the animals' choices than sites that carried little stimulus information.

Global and Local Choice-Related Signals in the LFP

LFPs recorded at different sites within the same cortical area can be strongly coherent (Leopold et al. 2003; Jia et al. 2011; Dubey and Ray 2016), suggesting that a prominent component of the LFP is common across sites. In addition, LFPs often show similar stimulus selectivity across recording sites. For instance, under some conditions, LFPs recorded millimeters apart share preference for stimulus orientation (Berens et al. 2008; Jia et al. 2011), color (Shirhatti and Ray 2018), and regions of visual space (Mineault et al. 2013). As a result, some have suggested that stimulus information in the LFP consists of a "local" component, often tuned similarly to the MUA, and a more "global" component that is common across sites (Jia et al. 2011; Mineault et al. 2013).

To assess the relative importance of global (i.e., common across sites) and local components, we decomposed the raw LFP into these two signals. The global component was defined as the mean LFP across all sites on each trial. Note that this definition is stringent: if there is a common signal with phase differences across sites, the mean signal would have much reduced amplitude. Indeed, we found that power in the global LFP was reduced roughly 25–300%, depending on frequency, relative to the average power available in each electrode. The local component was defined by subtracting the mean signal of the other electrodes on the array (i.e., a signal nearly identical to the global component) from each individual electrode on each trial. The local signal effectively involves re-referencing the LFP to the average signal across sites, similar to the average referencing scheme of Shirhatti et al. (2016).

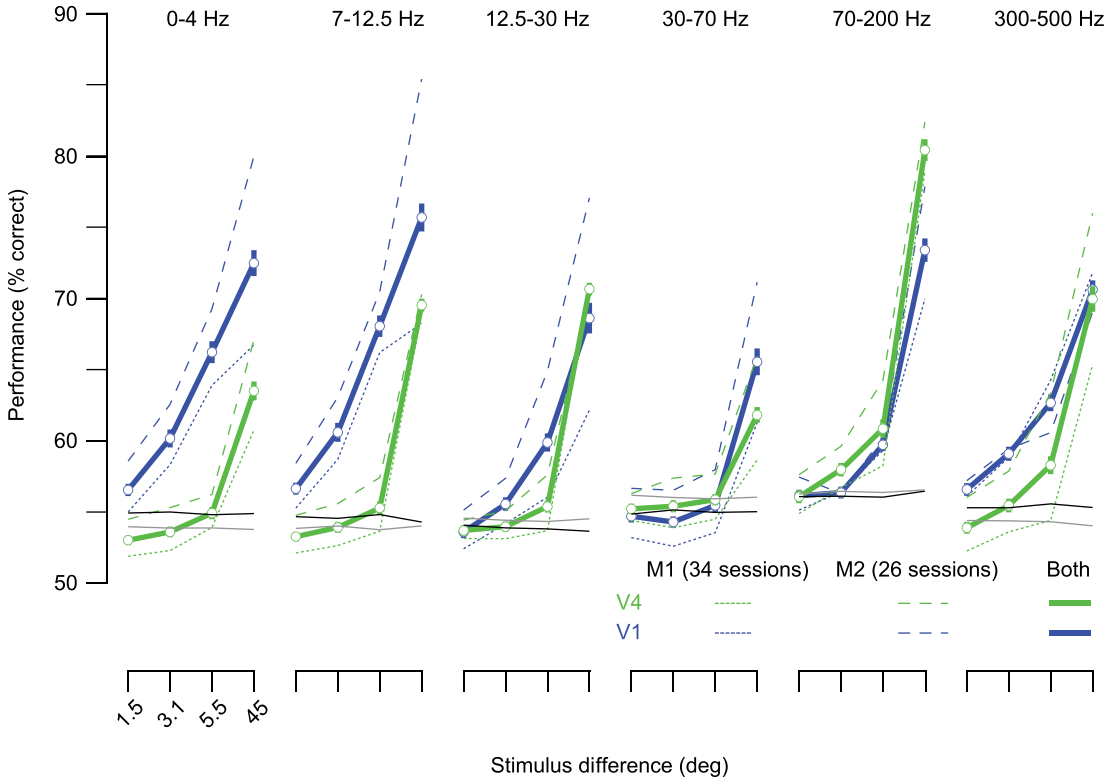

Figure 8. Stimulus decoding performance using the LFP. Each set of lines shows decoding performance (cross-validated) in discriminating between pairs of stimuli (abscissa), for a different frequency band. Conventions as in Figure 7.

We found clear choice information in the global LFP. We calculated absCP values using global LFP power on trials with vertical and horizontal choices. The absCP values were similar in magnitude to those calculated from the raw LFP (Fig. 10, compare to Fig. 4) and showed a similar dependence on epoch (strongest at the end of the trial), frequency (weakest in the gamma range), and area (stronger in V4 than V1). We confirmed that the choice information in the global LFP did not simply reflect a common stimulus-evoked transient response across electrodes. Similar choice information was available in the global-induced LFP, calculated after removing the stimulus-evoked potential (Supplementary Fig. 5).

To be sure that the global LFP did not simply reflect signal at a few dominant electrodes, we ranked electrodes based on their individual absCP magnitude, calculated from the raw LFP. We then calculated an average LFP (akin to the global LFP but not using all channels), separately for the half of channels with the strongest choice-signals and the half with the weakest. The magnitude of absCP for the average LFP derived from the weaker half of sites was substantially smaller than in stronger half, reduced by $53.6 \pm 3.5\%$ and $54.3 \pm 4.0\%$ in V1 and V4, respectively ($P < 0.01$ for all cases except high gamma, $P = 0.05$ in V4; no correction for multiple comparisons). If the average LFP reflected choice information in only a small subset of electrodes, we would expect a correlation near zero between the choice signals in the two subsets of data, since the weaker half of electrodes would not contain meaningful signal. However, the CP values for the average LFPs in the two subsets of data were highly correlated across all frequency bands (ranging between 0.85 and 0.91 for V4 and 0.65 and 0.94 for V1, in the epoch after stimulus offset). This correlation indicates substantial consistency of the average LFP in the two halves of the data set.

Next, we measured choice information present in the local signal. We found robust choice information in the local component of the LFP, evident both in the absCP values of individual electrodes (not shown) and in the performance of a population decoder (Fig. 11). In fact, performance was similar in most cases to the performance evident in the raw signal. We conclude that the LFP consists of global (common across electrodes) and local components, both of which contain information about animals' choices.

Discussion

We found that fluctuations in LFP power were predictive of animals' choices in a fine sensory discrimination task, on a trial-by-trial basis. Choice-related signals were most prominent in low and high frequencies and weakest in between in the gamma band. Choice signals in V4 were stronger and appeared sooner than in V1. LFPs were more informative of choice than spiking activity detected by the same electrodes. Finally, pooling LFP signals across electrodes provided little improvement over single electrode decoding, in part because much of the choice signal in the LFP appeared to be common across sites. Our results suggest that the LFP may be a useful and sensitive measure for assessing the relationship between neural activity and perceptual decisions.

Numerous studies have shown a correlation between perceptual decisions and neuronal spiking responses (Parker and Newsome 1998; Nienborg et al. 2012; Seidemann and Geisler

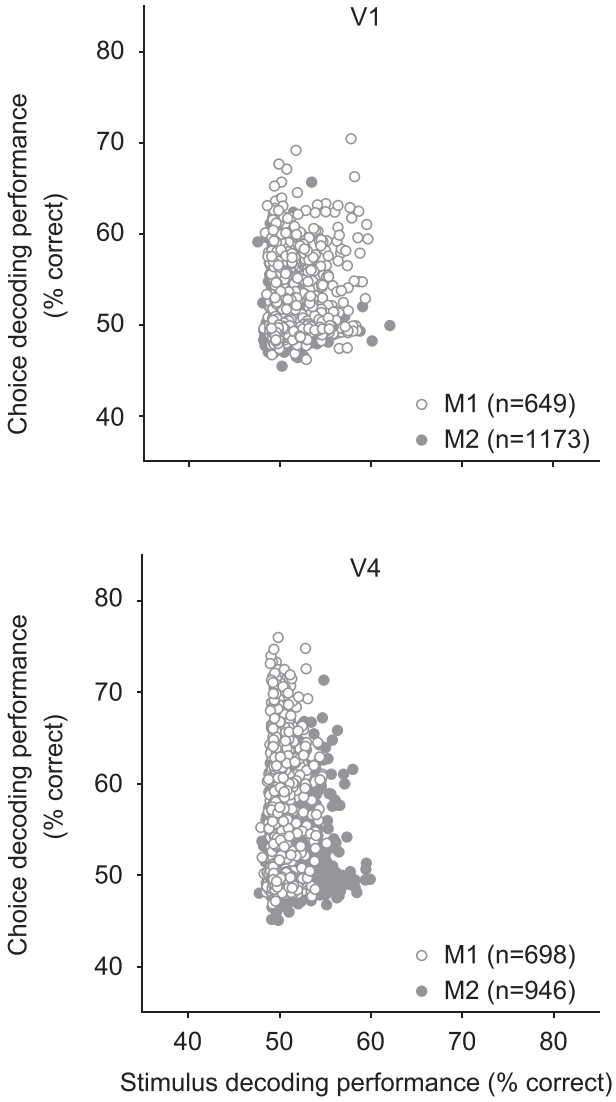

Figure 9. Relationship between stimulus and choice information, for V1 (top) and V4 (bottom). Each symbol indicates the performance for stimulus (abscissa) and choice (ordinate) decoding, using high-frequency LFP power (300–500 Hz) recorded at a single electrode. Stimulus decoding is performed for responses to the 45° grating compared with gratings offset by 5.5°. The difference in performance with Figure 8 arises because performance here is based on single electrodes rather than decoding all available electrodes. Open symbols show data from monkey 1; filled symbols from monkey 2.

2018). Two aspects of our findings are consistent with these spike-based studies of decision signals: LFP choice signals were stronger in V4 than V1 and appeared in V4 before V1. Differences in the magnitude of choice signals across stages of sensory processing have been inferred in previous studies (Nienborg et al. 2012). A similar difference in the magnitude, and in the dynamics of V1 and V4 choice signals, was evident in the spiking data recorded from these arrays (Jasper et al. 2019).

As in the spike-based analyses of Jasper et al. (2019), we found that choice signals were most evident after stimulus offset. These dynamics might indicate that our choice signals were related to the modulation of sensory responses by motor preparation (i.e., presaccadic modulation). However, presaccadic modulation of spiking activity begins roughly 100 ms before saccade onset (Tolias et al. 2001; Ibbotson and Krekelberg 2011), whereas choice signals were evident 200–400 ms before saccade initiation. In addition, presaccadic modulation of spiking activity is most evident when combined with visual drive (Tolias et al. 2001) and when saccades are made toward the RF (Super et al. 2004; Steinmetz and Moore 2010). In our study, choice signals were strongest in the absence of visual stimulation, and saccades were made to spatially offset targets. Thus, it seems unlikely that the dynamics of choice signals we observed can be ascribed to presaccadic modulation. It is worth noting that previous studies that used a brief stimulus presentation, as we did, also found a delay between sensory drive and the appearance of choice signals (Price and Born 2010; Smith et al. 2011, 2015).

Although there is a rich literature on decisions signals in spiking activity, there are only two studies, to our knowledge, that have assessed whether LFPs in macaque visual cortex contain decision-related information (Liu and Newsome 2006; Smith et al. 2015). Liu and Newsome (2006) recorded LFPs in area MT while animals performed a speed discrimination task. Consistent with our findings, they found robust choice-related signals across a broad range of frequencies. Unlike our study, however, they found that LFP-based CP values were correlated with those measured using MUA, whereas we found little relationship between the two signals. This discrepancy may be because the MUA used in their study aggregated signals from many neurons (peak firing rates were ~300 sp/s), and thus may have been a measure of local population activity, like the LFP. Our spiking measurements, on the other hand, involved recordings from single units or MUA consisting of a handful of units with clear spike waveforms (see Wissig and Kohn 2012, for comparison of our MUA recordings with well-isolated single units). Differences in the degree and the spatial extent of functional clustering—speed tuning in MT compared with orientation tuning in V1 and V4—might also contribute.

Smith et al. (2015) also studied the relationship between LFPs recorded in MT and animals' reports, in a motion detection task. They found robust detection-related signals in high (>100 Hz) and low (10–30 Hz, beta) frequency bands of the LFP. They also observed LFP-based decision signals for stimuli presented far away from the spatial RF of the recorded location. The authors argue that this signal might be related to fluctuations in attention, which would likely affect LFP power across a broad swath of MT and also alter detection performance. Because our study involved a discrimination task, the global component of the LFP is unlikely to be related to attentional fluctuations: a broad attention signal shared across neuronal preferences should not lead to more vertical or horizontal choices.

In our study, choice-related information in LFPs was frequency dependent, with several notable features. First, information was weakest in the gamma range. Previous work has proposed that gamma fluctuations are an integral component of cognition (Fries 2009). Some studies have found a relationship between trial-by-trial variations in gamma power and task performance (Shin and Moore 2019), between spike-field coherence in the gamma range and performance (Womelsdorf et al. 2008; Lee and Lisberger 2013), and between interareal gamma phase consistency and reaction times (Rohenkohl et al. 2018). However, we found that gamma power carried almost no information about the impending choice, unlike both higher and lower frequency components of the LFP (see also Liu and Newsome 2006; Smith et al. 2015). If gamma-band activity is integral to relaying

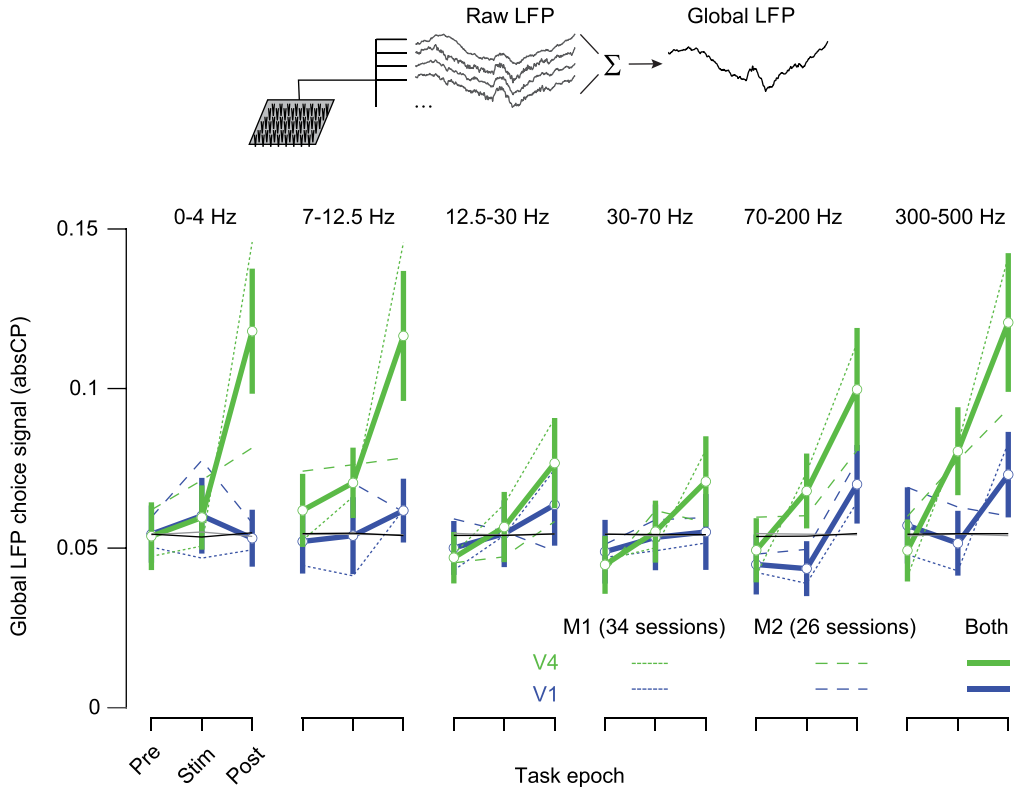

Figure 10. Choice information in the global LFP. The global LFP is calculated by summing the LFPs recorded on each electrode, on each trial (top). Each set of lines shows the absCP values, as a function of frequency band, area (V4 in green, V1 in blue), and task epoch (prestimulus, stimulus, and poststimulus). Dotted lines correspond to the data from monkey 1; dashed lines the data from monkey 2; solid lines show the aggregated data. Error bars (SEM) are shown only for the aggregate data to reduce clutter. Black line shows the 95th percentile of absCP values computed from the aggregate shuffled data for V1; gray line for the V4 data is identical.

signals to downstream areas (Fries 2009), then fluctuations in gamma power at a given recording site should be related to the efficacy with which local neuronal signals are relayed downstream (e.g., to higher visual or "decision" areas). The dissociation of gamma fluctuations from animals' choices suggests that gamma power is not closely related to perceptual decisions—a central aspect of sensory-based cognition—at least for our task (see also Rohenkohl et al. 2018). We note, however, that some work has suggested that gamma activity is enhanced by top-down influences, a process which may take a few hundred milliseconds to unfold (Richter et al. 2017). Because our task involved a brief stimulus presentation and a brief delay before animals signaled their choices, we cannot exclude the possibility that decision signals would be evident in gamma activity in a lengthier task.

Second, we found that choice-related signals in the alpha and beta components of the LFP were similar to those present in other frequency bands (such as 0–4 Hz or >70 Hz). Several studies have suggested that choice information in sensory cortex may arise primarily for top-down or feedback signals (Nienborg and Cumming 2009; Nienborg et al. 2012; Bondy et al. 2018; see also Yang et al. 2016 for work in rodent somatosensory cortex). Feedback signals have recently been ascribed to specific frequency bands, either in the alpha (5–15 Hz; van Kerkoerle et al. 2014; Michalareas et al. 2016) or beta range (14–18 Hz; Bastos et al. 2015). If choices reflect feedback and feedback information is especially evident in alpha or beta frequencies, one might expect that decision signals in early cortex would be strongest in this frequency range. This was not the case, perhaps indicating that inferring signal flow in the cortex based on power in specific frequency bands is excessively simplistic. Of course, we cannot exclude the possibility that recording in other cortical layers than those sampled by our implanted arrays would produce a different outcome, since the spectral composition of the LFP is layer specific (e.g., Maier et al. 2010; Xing et al. 2012; Smith et al. 2013; van Kerkoerle et al. 2014). Furthermore, because we estimated LFP power in relatively short epochs (200 ms) and smoothed across frequency bands using multiple tapers, our spectral resolution was limited. Thus, subtle differences between nearby frequencies might have gone undetected.

Third, we found that decisions could be predicted by the low frequency components of the LFP (0–4 Hz). Low frequency components are often found to be non-selective for visual stimuli (Henrie and Shapley 2005; Liu and Newsome 2006; Jia et al. 2011; Ray and Maunsell 2011; but see Belitski et al. 2008) and to be highly coherent across large cortical distances (Leopold et al. 2003; Jia et al. 2011). Nevertheless, these frequency components carried choice signals as robust as those present at high frequencies, which are typically stimulus selective (i.e., tuned) and often have preferences similar to local spiking activity (Liu and Newsome 2006; Berens et al. 2008; Jia et al. 2011; Ray and Maunsell 2011). It is unlikely that this low-frequency signal reflects the stimulus-locked transient (evoked potential). We found choice signals were strongest in the post-stimulus epoch, when the evoked LFP is weakest. Furthermore, removing this signal to isolate the induced LFP resulted in a similar pattern of results, including robust choice information at low frequencies (Supplementary Figs 1 and 5).

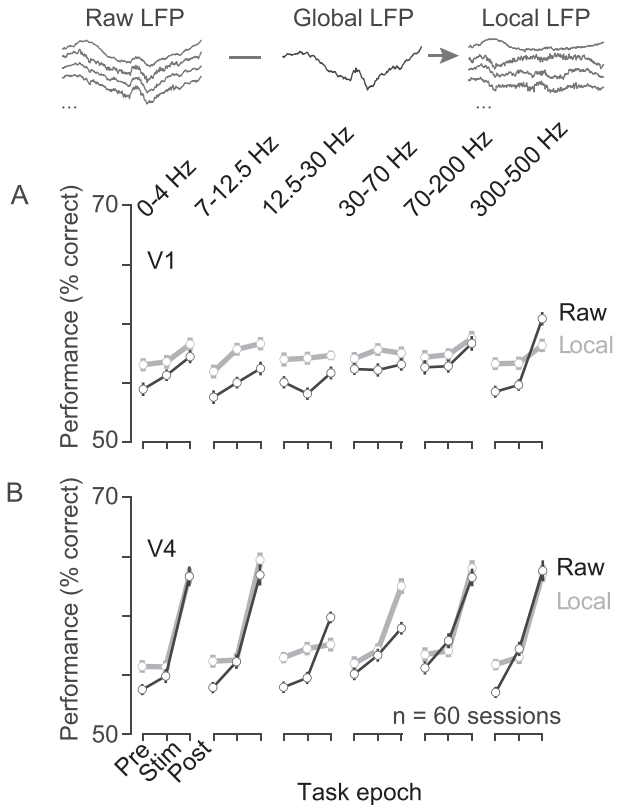

Figure 11. Choice decoding using local LFPs. (*A*) Decoding performance in V1 for raw LFPs (black; replotted from Fig. 7) and for local LFPs (gray; defined as the difference between the raw LFP recorded on each electrode and the average LFP recorded on all other electrodes). Conventions follow those of Figure 7. (*B*) Same as (*A*), but for V4. The number of cases is as reported in Figure 7.

A final notable aspect of our findings was the existence, particularly in V4, of a choice-related signal that was common across LFP sites—the "global" signal. The existence of a global decision-related LFP signal is consistent with previous work which has shown that LFPs recorded at nearby sites (i.e., up to several millimeters apart) can be highly coherent (Juergens et al. 1999; Frien and Eckhorn 2000; Leopold et al. 2003; Jia et al. 2011; Dubey and Ray 2016). This high coherence indicates that LFPs recorded millimeters apart are not independent signals and are thus likely to share some functional properties (e.g., decision information).

The source of this common signal is unclear. We were concerned that it might arise from our referencing scheme. However, both V1 and V4 arrays were referenced to a distant electrode (i.e., wire) that was placed on the surface of the brain, far from the arrays. If the global signal were introduced by referencing, the source of the reference signal would itself need to carry robust choice-related information, although the reference wire was not targeted to relevant sensory networks. Furthermore, under this explanation, the global signal in V1 and V4 should be similar, yet in both animals, the global signal was more robust in V4.

The global signal may instead reflect the volume conduction of either distant or locally generated signals. For instance, previous work has shown that intracranial recordings can reflect ocular EMG signals (Schomburg et al. 2014; Kovach et al. 2011; see also Parabucki and Lampl 2017). Thus, the global signal may reflect a distant activity source, strongly related to decisions, which is conducted to all of the recording electrodes (albeit more strongly to those in V4 than V1). Alternatively, the global signal might reflect the average of locally generated signals, which conduct freely between recording sites. If so, the existence of choice information in the global signal would require a bias in these aggregated signals so that, on average, more power would be present for one choice than another. Such a bias could arise from a slight imbalance (between choices) in the summed signals (Jia et al. 2011), akin to the orientation tuning evident in fMRI BOLD voxels which aggregate signals over a large volume of tissue (Norman et al. 2006). Given sufficient signal-to-noise, even a weak bias could provide substantial ability to predict decisions.

Although the use of the LFP to study perceptual decision-making is relatively rare, LFPs have been successfully used to read out local network representations. For instance, LFPs have been used to decode coarse motor commands such as the direction of a reach (Pesaran et al. 2002; Mehring et al. 2003). LFPs have also been shown to provide a correlate for the accumulation of sensory evidence in LIP cortex (Bollimunta and Ditterich 2012). At an even coarser scale, numerous studies have shown that perceptual reports of humans can be predicted by the amplitude or phase of various components of mass electrical (or magnetic) signals, such as those recorded in EEG, MEG, or electrocorticography (e.g., Donner et al. 2007, 2009; van Dijk et al. 2008; Busch et al. 2009; Foxe and Snyder 2011).

In this context, the presence of choice-related signal in the LFP in sensory cortex may not be surprising. However, we note that our study required decoding choice in a fine discrimination task. Nearby neurons often carry opposite choice signals (Nienborg et al. 2012): stronger responses in some neurons may indicate an increased likelihood of one choice, whereas stronger responses in nearby neurons are associated with a competing choice. Since the LFP can reflect the activity of neurons many hundreds of microns away, one might expect this spatial averaging would reduce or eliminate the information available about choice. Our results show that this is not the case. LFP power is usually more informative of choice than the spiking activity that we recorded. LFPs may thus be a useful and sensitive complement to spike-based analyses of choice signals.

Supplementary Material

Supplementary material can be found at *Cerebral Cortex* online.

Funding

National Institutes of Health (EY016774, EY028626); Irma T Hirchl Career Scientist Award.

Notes

We thank the members of the Kohn lab for assistance with the data collection; and Anna Jasper and Abhimanyu Pavuluri for helpful discussions. *Conflict of Interests*: The authors have no competing financial interests.

Authors' Contributions

S.T. and A.K. designed the study; S.T. performed the experiments; A.K. analyzed the data; A.K. and A.K. wrote the paper.

References

Andersen RA, Kellis S, Klaes C, Aflalo T. 2014. Toward more versatile and intuitive cortical brain-machine interfaces. *Curr Biol*. 24:R885–R897.

Bastos AM, Vezoli J, Bosman CA, Schoffelen JM, Oostenveld R, Dowdall JR, DeWeerd P, Kennedy H, Fries P. 2015. Visual areas exert feedforward and feedback influences through distinct frequency channels. *Neuron*. 85:390–401.

Belitski A, Gretton A, Magri C, Murayama Y, Montemurro MA, Logothetis NK, Panzeri S. 2008. Low-frequency local field potentials and spikes in primary visual cortex convey independent visual information. *J Neurosci*. 28:5696–5709.

Berens P, Keliris GA, Ecker AS, Logothetis NK, Tolias AS. 2008. Comparing the feature selectivity of the gamma-band of the local field potential and the underlying spiking activity in primate visual cortex. *Front Neurosci*. 2:2. doi: 10.3389/neuro.06.002.2008.

Bokil H, Andrews P, Kulkarni JE, Mehta S, Mitra PP. 2010. Chronux: a platform for analyzing neural signals. *J Neurosci Methods*. 192:146–151.

Bollimunta A, Ditterich J. 2012. Local computation of decision-relevant net sensory evidence in parietal cortex. *Cereb Cortex*. 22:903–917.

Bondy AG, Haefner RM, Cumming BG. 2018. Feedback determines the structure of correlated variability in primary visual cortex. *Nat Neurosci*. 21:598–606.

Britten KH, Newsome WT, Shadlen MN, Celebrini S, Movshon JA. 1996. A relationship between behavioral choice and the visual responses of neurons in macaque MT. *Vis Neurosci*. 13:87–100.

Busch NA, Dubois J, VanRullen R. 2009. The phase of ongoing EEG oscillations predicts visual perception. *J Neurosci*. 29:7869–7876.

Buzsáki G, Anastassiou CA, Koch C. 2012. The origin of extracellular fields and currents–EEG, ECoG, LFP and spikes. *Nat Rev Neurosci*. 13:407–420.

Chen Y, Geisler WS, Seidemann E. 2006. Optimal decoding of correlated neural population responses in the primate visual cortex. *Nat Neurosci*. 9:1412–1420.

Donner TH, Siegel M, Oostenveld R, Fries P, Bauer M, Engel AK. 2007. Population activity in the human dorsal pathway predicts the accuracy of visual motion detection. *J Neurophysiol*. 98:345–359.

Donner TH, Siegel M, Fries P, Engel AK. 2009. Buildup of choice-predictive activity in human motor cortex during perceptual decision making. *Curr Biol*. 19:1581–1585.

Dubey A, Ray S. 2016. Spatial spread of local field potential is band-pass in the primary visual cortex. *J Neurophysiol*. 116:1986–1999.

Einevoll GT, Kayser C, Logothetis NK, Panzeri S. 2013. Modelling and analysis of local field potentials for studying the function of cortical circuits. *Nat Rev Neurosci*. 14:770–785.

Foxe JJ, Snyder AC. 2011. The role of alpha-band brain oscillations as a sensory suppression mechanism during selective attention. *Front Psychol*. 2:154.

Frien A, Eckhorn R. 2000. Functional coupling shows stronger stimulus dependency for fast oscillations than for low-frequency components in striate cortex of awake monkey. *Eur J Neurosci*. 12:1466–1478.

Fries P. 2009. Neuronal gamma-band synchronization as a fundamental process in cortical computation. *Annu Rev Neurosci*. 32:209–224.

Gattass R, Sousa AP, Gross CG. 1988. Visuotopic organization and extent of V3 and V4 of the macaque. *J Neurosci*. 8:1831–1845.

Goris RLT, Ziemba CM, Stine GM, Simoncelli EP, Movshon JA. 2017. Dissociation of choice formation and choice-correlated activity in macaque visual cortex. *J Neurosci*. 37:5195–5203.

Haefner RM, Berkes P, Fiser J. 2016. Perceptual decision-making as probabilistic inference by neural sampling. *Neuron*. 90:649–660.

Hass CA, Horwitz GD. 2013. V1 mechanisms underlying chromatic contrast detection. *J Neurophysiol*. 109:2483–2494.

Henrie JA, Shapley R. 2005. LFP power spectra in V1 cortex: the graded effect of stimulus contrast. *J Neurophysiol*. 94:479–490.

Ibbotson M, Krekelberg B. 2011. Visual perception and saccadic eye movements. *Curr Opin Neurobiol*. 21:553–558.

Jasper AI, Tanabe S, Kohn A. 2019. Predicting perceptual decision using visual cortical population responses and choice history. *J Neurosci*. 39:6714–6727 ∗Equal contribution.

Jia X, Kohn A. 2011. Gamma rhythms in the brain. *PLoS Biol*. 9:2–5.

Jia X, Smith MA, Kohn A. 2011. Stimulus selectivity and spatial coherence of gamma components of the local field potential. *J Neurosci*. 31:9390–9403.

Jia X, Tanabe S, Kohn A. 2013. Gamma and the coordination of spiking activity in early visual cortex. *Neuron*. 77:762–774.

Juergens E, Guettler A, Eckhorn R. 1999. Visual stimulation elicits locked and induced gamma oscillations in monkey intracortical- and EEG-potentials, but not in human EEG. *Exp Brain Res*. 129:247–259.

Kajikawa Y, Schroeder CE. 2011. How local is the local field potential? *Neuron*. 72:847–858.

Katzner S, Nauhaus I, Benucci A, Bonin V, Ringach DL, Carandini M. 2009. Local origin of field potentials in visual cortex. *Neuron*. 61:35–41.

Kovach CK, Tsuchiya N, Kawasaki H, Oya H, Howard MA 3rd, Adolphs R. 2011. Manifestation of ocular-muscle EMG contamination in human intracranial recordings. *Neuroimage*. 54:213–233.

Kreiman G, Hung CP, Kraskov A, Quiroga RQ, Poggio T, DiCarlo JJ. 2006. Object selectivity of local field potentials and spikes in the macaque inferior temporal cortex. *Neuron*. 49: 433–445.

Lashgari R, Li X, Chen Y, Kremkow J, Bereshpolova Y, Swadlow HA, Alonso J-M. 2012. Response properties of local field potentials and neighboring single neurons in awake primary visual cortex. *J Neurosci*. 32:11396–11413.

Lee J, Lisberger SG. 2013. Gamma synchrony predicts neuron-neuron correlations and correlations with motor behavior in extrastriate visual area MT. *J Neurosci*. 33:19677–19688.

Leopold DA, Murayama Y, Logothetis NK. 2003. Very slow activity fluctuations in monkey visual cortex: implications for functional brain imaging. *Cereb Cortex*. 13:422–433.

Liu J, Newsome WT. 2006. Local field potential in cortical area MT: stimulus tuning and behavioral correlations. *J Neurosci*. 26:7779–7790.

Liu S, Gu Y, DeAngelis GC, Angelaki DE. 2013. Choice-related activity and correlated noise in subcortical vestibular neurons. *Nat Neurosci*. 16:89–97.

Maier A, Adams GK, Aura C, Leopold DA. 2010. Distinct superficial and deep laminar domains of activity in the visual cortex during rest and stimulation. *Front Syst Neurosci*. 10:4pii: 31. doi: 10.3389/fnsys.2010.00031.

Mäkelä P, Whitaker D, Rovamo J. 1993. Modelling of orientation discrimination across the visual field. *Vision Res*. 33: 723–730.

Mareschal I, Shapley RM. 2004. Effects of contrast and size on orientation discrimination. *Vision Res*. 44:57–67.

Mehring C, Rickert J, Vaadia E, De Oliveira SC, Aertsen A, Rotter S. 2003. Inference of hand movements from local field potentials in monkey motor cortex. *Nat Neurosci*. 6:1253–1254.

Michalareas G, Vezoli J, van Pelt S, Schoffelen JM, Kennedy H, Fries P. 2016. Alpha-beta and gamma rhythms subserve feedback and feedforward influences among human visual cortical areas. *Neuron*. 89:384–397.

Mineault PJ, Zanos TP, Pack CC. 2013. Local field potentials reflect multiple spatial scales in V4. *Front Comput Neurosci*. 26(7):21.

Nienborg H, Cumming BG. 2006. Macaque V2 neurons, but not V1 neurons, show choice-related activity. *J Neurosci*. 26:9567–9578.

Nienborg H, Cumming BG. 2009. Decision-related activity in sensory neurons reflects more than a neurons causal effect. *Nature*. 459:89–92.

Nienborg H, Cohen MR, Cumming BG. 2012. Decision-related activity in sensory neurons: correlations among neurons and with behavior. *Annu Rev Neurosci*. 35:463–483.

Norman KA, Polyn SM, Detre GJ, Haxby JV. 2006. Beyond mind-reading: multi-voxel pattern analysis of fMRI data. *Trends Cogn Sci*. 10:424–430.

Parabucki A, Lampl I. 2017. Volume conduction coupling of whisker-evoked cortical LFP in the mouse olfactory bulb. *Cell Rep*. 21:919–925.

Parker AJ, Newsome WT. 1998. Sense and the single neuron: probing the physiology of perception. *Annu Rev Neurosci*. 21:227–277.

Pesaran B, Pezaris JS, Sahani M, Mitra PP, Andersen RA. 2002. Temporal structure in neuronal activity during working memory in macaque parietal cortex. *Nat Neurosci*. 5:805–811.

Pitkow X, Liu S, Angelaki DE, DeAngelis GC, Pouget A. 2015. How can single sensory neurons predict behavior? *Neuron*. 87:411–423.

Price NS, Born RT. 2010. Timescales of sensory- and decision-related activity in the middle temporal and medial superior temporal areas. *J Neurosci*. 30:14036–14045.

Purushothaman G, Bradley DC. 2005. Neural population code for fine perceptual decisions in area MT. *Nat Neurosci*. 8:99–106.

Qian J, Hastie T, Friedman J, Tibshirani R, Simon N (2013) *Glmnet for MATLAB*. http://www.stanford.edu/~hastie/glmnet_matlab/

Ray S, Maunsell JHR. 2011. Different origins of gamma rhythm and high-gamma activity in macaque visual cortex. *PLoS Biol*. 9:e1000610.

Ray S, Maunsell JH. 2015. Do gamma oscillations play a role in cerebral cortex? *Trends Cogn Sci*. 19:78–85.

Richter CG, Thompson WH, Bosman CA, Fries P. 2017. Top-down beta enhances bottom-up gamma. *J Neurosci*. 37:6698–6711.

Rohenkohl G, Bosman CA, Fries P. 2018. Gamma synchronization between V1 and V4 improves behavioral performance. *Neuron*. 100:953–963.

Schoups AA, Vogels R, Orban GA. 1995. Human perceptual learning in identifying the oblique orientation: retinotopy, orientation specificity and monocularity. *J Physiol*. 483:797–810.

Seidemann E, Geisler WS. 2018. Linking V1 activity to behavior. *Annu Rev Vis Sci*. 4:287–310.

Schomburg EW, Fernández-Ruiz A, Mizuseki K, Berényi A, Anastassiou CA, Koch C, Buzsáki G. 2014. Theta phase segregation of input-specific gamma patterns in entorhinal-hippocampal networks. *Neuron*. 84:470–485.

Shin H, Moore CI. 2019. Persistent gamma spiking in SI nonsensory fast spiking cells predicts perceptual success. *Neuron*. 103:1150–1163.

Shiozaki HM, Tanabe S, Doi T, Fujita I. 2012. Neural activity in cortical area V4 underlies fine disparity discrimination. *J Neurosci*. 32:3830–3841.

Shirhatti V, Borthakur A, Ray S. 2016. Effect of reference scheme on power and phase of the local field potential. *Neural Comput*. 28:882–913.

Shirhatti V, Ray S. 2018. Long-wavelength (reddish) hues induce unusually large gamma oscillations in the primate primary visual cortex. *Proc Natl Acad Sci U S A*. 115:4489–4494.

Smith JE, Zhan CA, Cook EP. 2011. The functional link between area MT neural fluctuations and detection of a brief motion stimulus. *J Neurosci*. 31:13458–13468.

Smith JE, Beliveau V, Schoen A, Remz J, Zhan CA, Cook EP. 2015. Dynamics of the functional link between area MT LFPs and motion detection. *J Neurophysiol*. 114:80–98.

Smith MA, Jia X, Zandvakili A, Kohn A. 2013. Laminar dependence of neuronal correlations in visual cortex. *J Neurophysiol*. 109:940–947.

Steinmetz NA, Moore T. 2010. Changes in the response rate and response variability of area V4 neurons during the preparation of saccadic eye movements. *J Neurophysiol*. 103:1171–1178.

Super H, van der Togt C, Spekreijse H, Lamme VA. 2004. Correspondence of presaccadic activity in the monkey primary visual cortex with saccadic eye movements. *Proc Natl Acad Sci U S A*. 101:3230–3235.

Tolias AS, Moore T, Smirnakis SM, Tehovnik EJ, Siapas AG, Schiller PH. 2001. Eye movements modulate visual receptive fields of V4 neurons. *Neuron*. 29:757–767.

Uka T, DeAngelis GC. 2004. Contribution of area MT to stereoscopic depth perception: choice-related response modulations reflect task strategy. *Neuron*. 42:297–310.

van Dijk H, Schoffelen JM, Oostenveld R, Jensen O. 2008. Prestimulus oscillatory activity in the alpha band predicts visual discrimination ability. *J Neurosci*. 28:1816–1823.

Van Essen DC, Newsome WT, Maunsell JHR. 1984. The visual field representation in striate cortex of the macaque monkey: asymmetries, anisotropies, and individual variability. *Vision Res*. 24:429–448.

van Kerkoerle T, Self MW, Dagnino B, Gariel-Mathis M-A, Poort J, van der Togt C, Roelfsema PR. 2014. Alpha and gamma oscillations characterize feedback and feedforward processing in monkey visual cortex. *Proc Natl Acad Sci*. 111:14332–14341.

Xing D, Yeh C-I, Shapley RM. 2009. Spatial spread of the local field potential and its laminar variation in visual cortex. *J Neurosci*. 29:11540–11549.

Xing D, Yeh CI, Burns S, Shapley RM. 2012. Laminar analysis of visually evoked activity in the primary visual cortex. *Proc Natl Acad Sci USA*. 109:13871–13876.

Wissig SC, Kohn A. 2012. The influence of surround suppression on adaptation effects in primary visual cortex. *J Neurophysiol*. 107:3370–3384.

Womelsdorf T, Fries P, Mitra PP, Desimone R. 2008. Gamma-band synchronization in visual cortex predicts speed of change detection. *Nature*. 439:733–736.

Yang H, Kwon SE, Severson KS, O'Connor DH. 2016. Origins of choice-related activity in mouse somatosensory cortex. *Nat Neurosci*. 19:127–134.

Zanos TP, Mineault PJ, Pack CC. 2011. Removal of spurious correlations between spikes and local field potentials. *J Neurophysiol*. 105:474–486.